Hindawi Publishing Corporation
Journal of Nanomaterials
Volume 2015, Article ID 985872, 9 pages
http://dx.doi.org/10.1155/2015/985872

Research Article

Synthesis Method Effect of $CoFe_2O_4$ on Its Photocatalytic Properties for H_2 Production from Water and Visible Light

Yudith Ortega López,[1] Hugo Medina Vázquez,[2] Jesús Salinas Gutiérrez,[1] Vanessa Guzmán Velderrain,[1] Alejandro López Ortiz,[1] and Virginia Collins Martínez[1]

[1]*Laboratorio Nacional de Nanotecnología, Departamento de Materiales Nanoestructurados, Centro de Investigación en Materiales Avanzados S. C., Miguel de Cervantes 120, 31109 Chihuahua, CHIH, Mexico*
[2]*Facultad de Ciencias Químicas, Universidad Autónoma de Chihuahua, Campus Universitario No. 2, 31125 Chihuahua, CHIH, Mexico*

Correspondence should be addressed to Virginia Collins Martínez; virginia.collins@cimav.edu.mx

Received 11 October 2014; Revised 20 December 2014; Accepted 24 December 2014

Academic Editor: Zhenyi Zhang

Copyright © 2015 Yudith Ortega López et al. This is an open access article distributed under the Creative Commons Attribution License, which permits unrestricted use, distribution, and reproduction in any medium, provided the original work is properly cited.

Currently, the need for more efficient materials that work in the visible light spectrum for hydrogen production has been increasing. Under this criterion, ferrites are ideal because their energetic properties are favorable to photocatalysis as they have a low band gap (1.5 to 3 ev). In this particular research, ferrite is presented as a hydrogen producer. Cobalt ferrites were synthesized by chemical coprecipitation (CP) and ball milling (BM) for comparison of their performance. The characterization of the materials was carried out with X-ray diffraction (XRD), scanning electron microscopy (SEM), transmission electron microscopy (TEM), BET surface area, UV-VIS spectroscopy, and water adsorption/desorption tests. Evaluation of the photocatalytic activity under visible light was followed by gas chromatography. The results showed that cobalt ferrite by ball milling had a higher photocatalytic activity; this is attributed to the vacancies generated during the milling process at which the sample was exposed.

1. Introduction

Recently, hydrogen has received considerable attention as a next generation energy carrier. While several technologies can be used to generate hydrogen, only some of them can be considered environmentally friendly. There is a general perception that hydrogen is obtained through clean technologies, but this may not be necessarily true. If hydrogen is produced from natural gas (steam reforming), coal, or biomass (gasification), a large amount of energy is used, not to mention a substantial amount of CO_2 generated as a byproduct. In order to avoid the CO_2 generation and a high energy consumption during hydrogen production, the splitting of the water molecule, together with the use of an alternative source of energy like hydraulic, wind or solar can be considered as the best option to produce hydrogen. From these alternative energies, solar is the most promising approach, since limitations related to the required space are less demanding.

Hydrogen production via the splitting of the water molecule using solar energy can generally be classified into three types: thermochemical, photobiological, and photocatalytic. The principle of the water splitting is thermochemically achieved using concentrators to collect heat from the sun, which can normally reach about 2000°C, and using the collected heat to carry out the dissociation reaction of the water molecule in the presence of a catalyst such as ZnO [1–5]. Although this technique seems to be unsophisticated, the management/heat control and the quest for heat resistant materials have become a major challenge. In addition, high concentration solar systems are essential to achieve the requirement of high temperature, which makes this technique often expensive.

The photobiological water splitting [6–8] can be divided into two groups based on the selected microorganisms, the generated products, and the reaction mechanisms involved. Hydrogen production by oxygenic photosynthetic cyanobacteria or green algae under irradiation of light and anaerobic

conditions is referred to as water biophotolysis, while producing hydrogen for anoxygenic photosynthetic bacteria under light irradiation conditions is known as anaerobic organic biophotolysis.

Despite the fact that water biophotolysis is a "clean" way to produce hydrogen, this still has several problems waiting to be solved, including low hydrogen yield, enzymes poisoning by the presence of oxygen, and the difficulty in design and scaling of a bioreactor for the process.

Moreover, the photocatalytic splitting of the water molecule is another promising technology to produce "clean" hydrogen. Compared to the thermochemical and photobiological process, this technology has the following advantages: the low cost of the process and the ability to separate the hydrogen and oxygen evolution during the reaction and suitable systems for domestic applications with small reactors, thus providing a huge market potential.

Currently, TiO_2 is the most common and widely studied photocatalyst. This is because of its high stability and photocorrosion resistance, a phenomenon that occurs with most common semiconductor materials that can be used. However, their efficiency is very low and the process is limited to the use of high-energy radiation (UV) sources. Radiation of these characteristics can only be provided from artificial mechanisms with the consequent energy expenditure, because the UV light occupies only 4% of the sunlight, which is a limiting factor for the photocatalytic technology using TiO_2 as a catalyst.

This process for hydrogen production is unique in the sense that it is generated from solar energy, which would become a large clean and economic path for energy generation.

It is in this sense that the search for a photocatalyst activated under solar radiation (visible light occupies 43% of the solar spectrum) and highly effective becomes one of the most important challenges in this technology.

One of the synthetic methods used for the preparation of photocatalysts is the coprecipitation technique, as it helps in obtaining a powder precursor of high homogeneity, by precipitation of intermediates (typically hydroxides or oxalates), so it is an economical synthesis technique. Another easy access and low cost synthesis method is by mechanical milling, which uses more available raw materials, and cheaper than other methods [9, 10]. Mechanical milling processes not only can produce an alloy but also can cause chemical reactions, besides obtaining nanometric size particles [11].

Ferrites are viable alternative materials to TiO_2 to be used as photocatalysts for hydrogen production; transition metal ferrites have a number of advantages, mainly emphasizing their low cost, effective catalytic activity, corrosion resistance, and most importantly their wide band gap into the visible light spectrum [12–14]. The selection of these materials is based on the redox activity and especially their ability to store oxygen in its crystalline lattice. Ferrites have a tendency, when burned under reducing atmospheres, to form compounds with oxygen defects, which facilitates the fixation of oxygen in the existing vacancies. Therefore, these materials are excellent candidates for the production of hydrogen from water, while providing the solar energy needed for the process.

Therefore, the main objective of this study is to synthesize cobalt ferrites by chemical coprecipitation (CP) and mechanical milling (BM) and to determine the effect of the synthesis method on the ferrite photocatalytic activity towards the production of hydrogen.

2. Materials and Methods

2.1. Synthesis. $CoFe_2O_4$ spinel was prepared by coprecipitation (CP) starting from nitrate precursors and modifying the procedure reported by Hu et al. [15]. In this method $Fe(NO_3)_3{\cdot}9H_2O$ and $Co(NO_3)_2{\cdot}6H_2O$ solutions were added to NaOH as a precipitating agent. The obtained precipitate was filtered and washed to remove any sodium residue. Thereafter, the residue was dried and placed in an agate mortar to obtain a fine and homogeneous powder. Nanosized crystalline oxide powder was obtained by exposing this to a moderate heat treatment at 250°C by 6 hours, followed by 1 h at 350°C.

For the preparation of CoF_2O_4 particles by the mechanical milling (BM) technique, the procedure consisted of employing metallic Fe and Co_3O_4 as precursors in a molar ratio of 2 : 1. Once the material was in stoichiometric amounts, this was mixed and exposed to 700°C by 4 hours. Subsequently, in order to both obtain the desired spinel phase and reduce particle size, the sample was subjected to mechanical milling with an effective time of 12 hours. The milling was carried out in a Spex CertiPrep 8000M Mixer/Mill, using a weight ratio of balls (0.7 cm) to powder ($B : P_w$) of 10 : 1. To perform this synthesis a D2 steel vial was manufactured and exposed to a heat treatment; this consisted of an austenitizing temperature of 1010°C, oil quenching, and tempering at a temperature varying from 300 to 400°C.

In order to determine the temperatures to be used during the calcination of the samples thermogravimetric analyses were carried out from powders obtained during each synthesis. These analyses were performed in a TGA Instrument TA Q500, using an initial sample weight of about 14 to 15 mg placed in a platinum crucible and employing a heating rate of 10°C/min from room temperature to 980°C under an air flow.

2.2. Characterization. Characterization of the samples was performed by X-ray diffraction (XRD) using a PANalytical X'Pert PRO diffractometer with X'Celerator model detector, scanning electron (SEM), and transmission (TEM) microscopy using a JSM-7401F and a Philips model CM-200, respectively. BET surface area was determined by employing an Autosorb-1 equipment and UV-Vis spectroscopy on a Perkin Elmer lambda 10 model.

The water vapor adsorption/desorption tests were performed by TGA. These tests were achieved by heating about 14 to 15 mg of sample at 130°C under a nitrogen flow (100 cm^3/min) for 20 minutes to clean the sample surface and followed by an isotherm at 35°C to monitor the water adsorption/desorption behavior in a TA Instrument Q500 TGA. In order to evaluate the presence of oxygen vacancies within each sample, TGA reductions were made using a 5% H_2/N_2 and a flow rate of 100 cm^3/min, at a heating rate of 10°C/min from room temperature to 750°C.

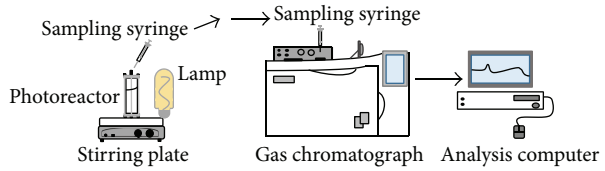

Figure 1: Photocatalytic experimental evaluation setup for the suspension; 0.2 gr of $CoFe_2O_4$, H_2O, and CH_3OH (sacrificial agent).

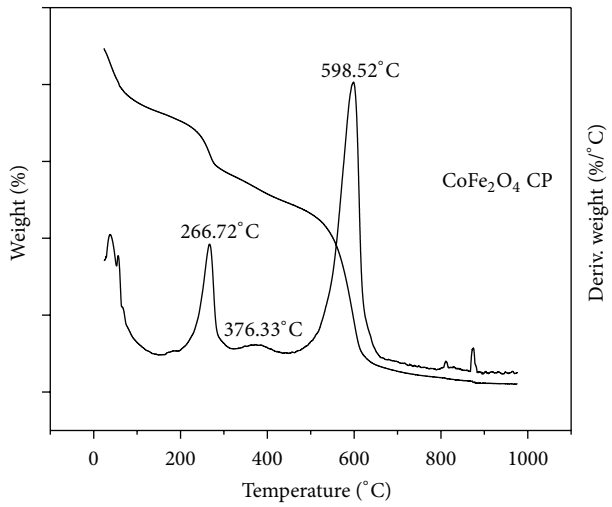

Figure 2: TGA of the precipitate to synthesize $CoFe_2O_4$ CP sample.

Photocatalytic ferrites were evaluated by splitting of the water molecule, using a 250 W mercurial lamp and adding methanol to the water reactor system as sacrificial agent (2% vol). The reaction was monitored by gas chromatography using a gas chromatograph (GC) Perkin Elmer Clarus 500. The system setup employed for carrying out the photocatalytic evaluation of the materials is presented in Figure 1. This system is composed of a photoreactor, artificial lighting, and GC analysis equipped with a personal computer data collection.

In order to monitor the photocatalytic reaction, gas samples were taken at regular time intervals using a 1 mL syringe for gases through a septum located at the upper section of the photoreactor. A sample under darkness was taken at the initial concentration and then the sampling took place every hour up to a total of 8 hours of irradiation.

3. Results and Discussions

3.1. Thermogravimetric Analysis. Determination of the heat treatment temperature of the precipitate product for sample $CoFe_2O_4$ CP during its synthesis was found using a temperature scan through thermogravimetric analysis. Figure 2 presents ($CoFe_2O_4$ CP) two signals, both with respect to temperature: one for the weight loss of the sample and the second for the derivative of this. In this figure, two slight slope changes at 267 and 350°C can be observed. In both cases, the small slopes observed are indicative of slow kinetics.

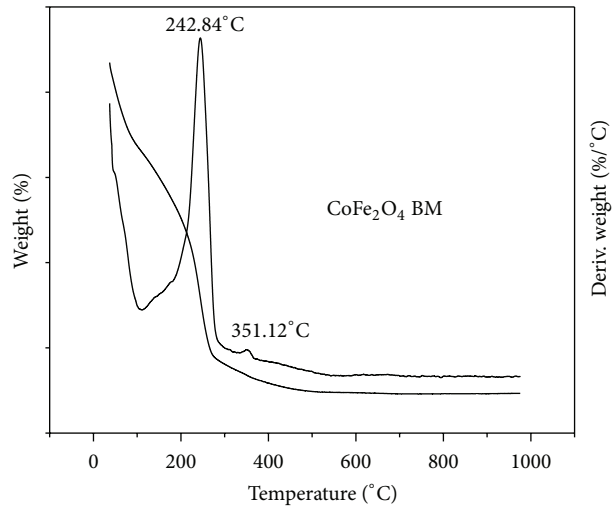

Figure 3: Thermogram for sample $CoFe_2O_4$ BM.

These results were used to establish the temperature and time of heat treatment for this sample. This treatment consisted of keeping the sample for 6 hours at 250°C and 1 h at 350°C; this was set in order to achieve the $CoFe_2O_4$ spinel phase, while maintaining a nanometric particle size in the sample; the slower kinetics is compensated by providing a prolonged heat treatment time (6 hours) [16].

In the case of the $CoFe_2O_4$ BM sample, determination of the calcination temperature of the Fe and Co_3O_4 mixture was established according to a thermogravimetric analysis. Figure 3 shows the thermogram of the Fe and Co_3O_4 mixture in a stoichiometric ratio ($CoFe_2O_4$ BM), where it is clear that at 700°C the sample is thermally stable [17]. From the above analysis, it was established that the heat treatment was set to 700°C by 4 hours. Subsequently, the sample was exposed to a mechanical milling process for 12 hours of effective time.

3.2. X-Ray Diffraction (XRD). Figure 4 presents the X-ray diffraction pattern for the synthesized sample by chemical coprecipitation, as well as for sample prepared by mechanical milling, $CoFe_2O_4$ CP and $CoFe_2O_4$ BM, respectively. Programs from the Diffrac-Plus package (Bruker AX Systems) were used for the data processing, including the "Search/Match" identification tool, using the PDF-2 database (ICDD, 2002) ICDD PDF-2 on CD-ROM, Rls 2002, International Centre for Diffraction Data, Pennsylvania, 2002. Analysis of the diffraction patterns indicates that both materials are crystalline, prevailing the $CoFe_2O_4$ spinel phase. However, for the case of the ferrite obtained by chemical coprecipitation, the Fe_2O_3 phase was also detected; nevertheless, some of the signals from this phase overlap with the $CoFe_2O_4$ phase. This result can be explained considering the phase diagram of Fe-Co-O_2 system (P = 1 atm, T = 300–1400°C). This result can be explained considering phase diagram of the Fe-Co-O_2 system at lower temperatures than 1400◦C, atmospheric pressure, and stoichiometric ratios of Co and Fe ions, which predicts that the solid will consist of a mixture of cobalt ferrite and hematite (Fe_2O_3). The phase

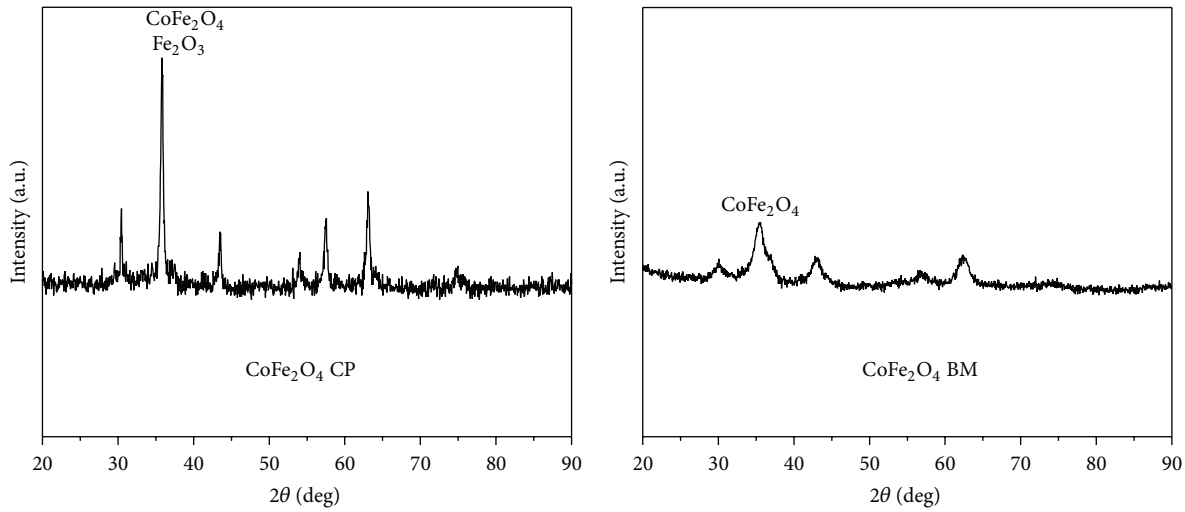

Figure 4: XRD patterns for $CoFe_2O_4$CP (a) and $CoFe_2O_4$ BM (b) samples.

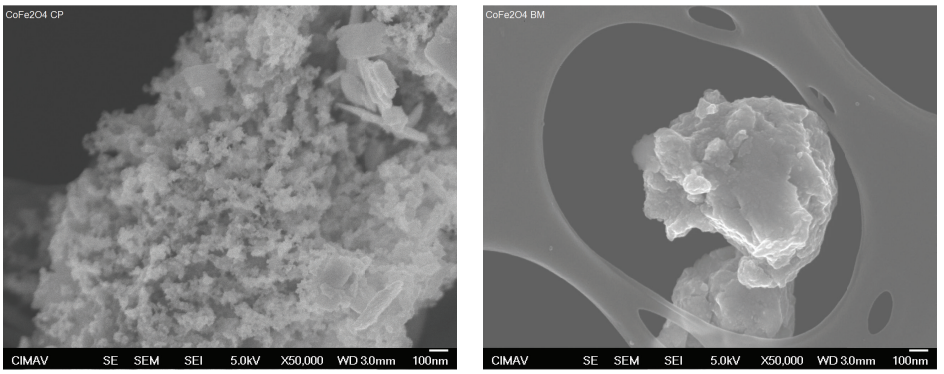

Figure 5: SEM from samples $CoFe_2O_4$CP (a) and $CoFe_2O_4$BM (b).

diagram predicts that the solid will consist of a mixture of cobalt ferrite and hematite (Fe_2O_3).

For the sample $CoFe_2O_4$ BM, where the initial mixture of metallic Fe and Co oxide is exposed to energetic conditions such as high temperature and impact, cobalt ferrite spinel is readily possible [18].

From X-ray patterns information and through the Scherrer equation, it was possible to calculate the crystal sizes of the materials. The sample $CoFe_2O_4$ CP presents a crystal size of about 20 nm while $CoFe_2O_4$ BM sample exhibits a crystal size of around 5 nm, which is extremely smaller than that of the $CoFe_2O_4$ CP sample. These results are expected, since, by comparing the width of the peaks of both diffraction patterns, it can be clearly seen that the broadening increase of the XRD peaks for the $CoFe_2O_4$ BM sample, consistent with a decrease of the crystal size, unlike the pattern for the $CoFe_2O_4$ CP sample, presents narrow and sharp peaks, indicative of a larger crystal size.

3.3. Scanning and Transmission Electron Microscopy. Scanning and transmission electron microscopy were used to determine the morphology and particle size of the samples under study. Figure 5 shows SEM images for samples $CoFe_2O_4$ CP and $CoFe_2O_4$ BM showing that both materials are formed of irregularly shaped agglomerates. In Figure 5, $CoFe_2O_4$ CP (a) shows the presence of two morphologies. The first is formed by agglomerated nanoparticles, which corresponds to the spinel phase, and the second is composed by plate-shaped particles of larger size that corresponds to hematite while sample $CoFe_2O_4$ BM (b) is formed by large agglomerates, which are composed of particles presenting clear evidence of sintering, and is attributed to the high temperature employed during the synthesis process (700°C).

Figure 6 shows TEM images of the synthesized cobalt ferrite samples, while by analyzing the image for $CoFe_2O_4$ CP sample a particle size of around 25 nm can be estimated. This behavior can be associated with the control of the precipitate formation during the synthesis process, which is achieved by a strict flow regulation of the precursor's solutions (both of Co and Fe). Controlled flow induces a slow kinetics behavior for particle nucleation and growth, which makes particles reach nanometer sizes. Comparing the above results with those

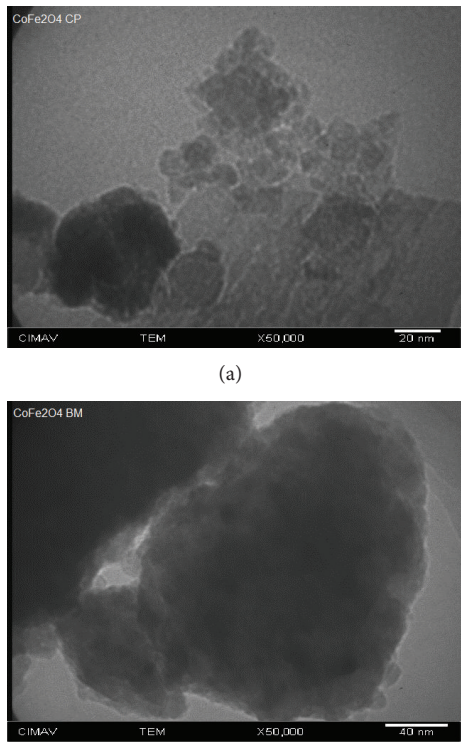

Figure 6: TEM image for samples $CoFe_2O_4$CP (a) and $CoFe_2O_4$BM (b).

reported by Zi et al. [19] (who also synthesized cobalt ferrite by coprecipitation) it was found that research, which reported powders with a particle size between 20 and 30 nm, showed very similar behavior to sample $CoFe_2O_4$ CP.

Moreover, in Figure 6 it can be seen that sample $CoFe_2O_4$ BM exhibits highly compact agglomerates (where the ultrasonic process was not effective to disperse the sample) with sizes between 100 and 500 nm, and these formed by particles of about 20 nm that apparently were fused together. The formation of these densified agglomerates is associated with the exposure of the material to the synthesis temperature of 700°C, confirming the results observed by SEM. However, this sample is nanocrystalline (according to XRD results) and these highly densified agglomerates tend to behave as a particulate material.

3.4. BET Surface Area (Brunauer, Emmett, and Teller) and Adsorption Isotherms. Values of specific surface areas for the photocatalyst synthesized by chemical coprecipitation and mechanical milling were 20 and 4 m^2/g, respectively. These values can be explained from particle size results determined by transmission electron microscopy.

Sample $CoFe_2O_4$ CP that corresponds to a particle size of 25 nm presented a higher surface area (20 m^2/g) compared to sample $CoFe_2O_4$ BM, which exhibited significantly large particles (agglomerates), ranging from 100 to 500 nm, which results in a surface area of only 4 m^2/g. The decreasing trend in the specific surface area of materials subjected to mechanical milling can be attributed to a strong aggregation between particles promoted by intensive milling, as reported by Cedeño-Mattei et al. [20].

Figure 7 shows adsorption isotherms for samples $CoFe_2O_4$ CP and $CoFe_2O_4$ BM, where it can be seen that both samples show no hysteresis, suggesting that these samples are nonporous solids. These results are expected since mechanical milling and coprecipitation synthesis methods generally produce nonporous materials.

3.5. UV/Vis Spectroscopy. Figure 8 presents the UV/Vis diffuse reflectance spectra for samples $CoFe_2O_4$ CP and $CoFe_2O_4$ BM for an indirect transition employing the Tauc model.

These spectra clearly show that values of the energy of the forbidden band are within the visible light spectrum for both cases. The reflectance values were converted in terms of absorption through the Kubelka-Munk function ($F(R)$) to determine the forbidden bandwidth by extrapolating the linear portion to the abscissa, obtaining band gap energy values of 1.38 eV for $CoFe_2O_4$ CP and 1.15 eV for $CoFe_2O_4$ BM. Authors like Limei et al. [21] reported very similar values (~1.5 eV) to those obtained experimentally. This behavior can be explained with findings reported by Chavan et al. [22], who found that the band gap is highly dependent on the particle size; as the particle size of a ferrite type semiconductor increases, its forbidden band decreases, and vice versa. Therefore, by comparing the band gap values between the studied samples, it is expected that the $CoFe_2O_4$ CP sample presents a greater band gap (1.38 eV) than sample $CoFe_2O_4$ BM (1.15 eV). This is because $CoFe_2O_4$ CP is formed by particles of 25 nm size, whereas this is opposite for the case of sample $CoFe_2O_4$ BM where the particle size (agglomerates) is significantly higher (100–500 nm).

3.6. Water Adsorption and Desorption (Gravimetric Method). Figure 9 shows graphs of water adsorption/desorption gravimetric isotherms of the synthesized materials. Comparing the water adsorption/desorption capacities of both materials it can be observed that there is a significant difference between the $CoFe_2O_4$ CP sample and the sample synthesized by mechanical milling ($CoFe_2O_4$ BM).

Figure 9 shows a thermogravimetric isotherm plot for the adsorption/desorption of water of synthesized ferrites ($CoFe_2O_4$ CP and $CoFe_2O_4$ BM). Comparing the capacities of both materials, sample $CoFe_2O_4$ CP presented around the double H_2O adsorption/desorption capacity with respect to sample $CoFe_2O_4$ BM synthesized by mechanical milling. The water adsorption from the sample synthesized by coprecipitation was about 39 mgH_2O/g, while the sample obtained by mechanical milling had 30 mgH_2O/g. These results are interesting in the sense that if a comparison is made in terms of water adsorption per surface area, it results in a greater water adsorption capacity for the sample synthesized by mechanical milling with 7.5 mgH_2O/m^2 compared to 1.95 mgH_2O/m^2 of sample synthesized by coprecipitation.

This difference in water adsorption capacity can be associated with vacancies present in the $CoFe_2O_4$ BM sample due

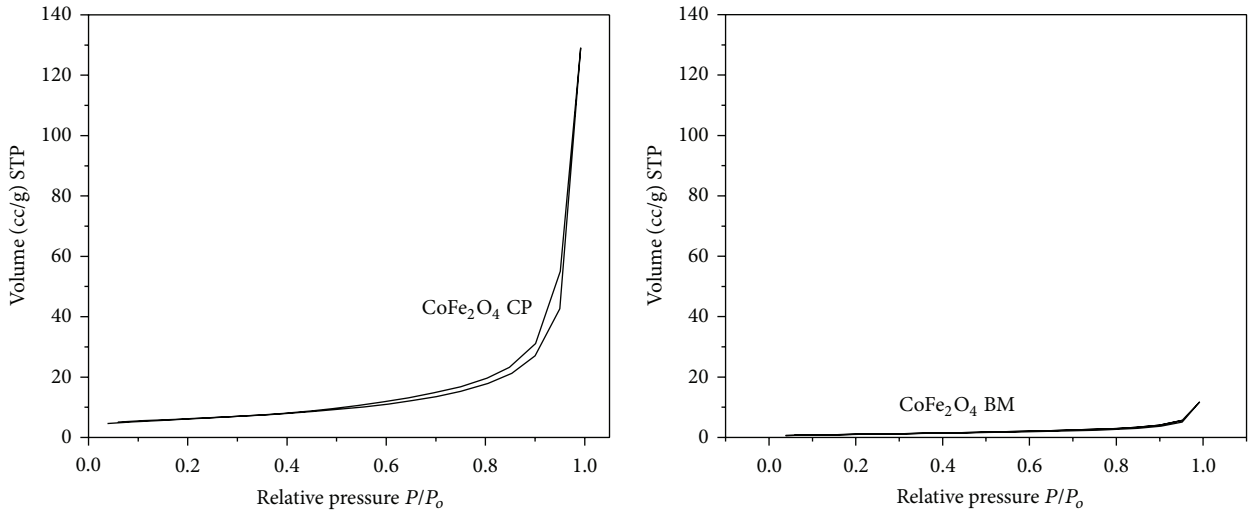

FIGURE 7: N_2 adsorption isotherms for $CoFe_2O_4$ CP and $CoFe_2O_4$BM samples.

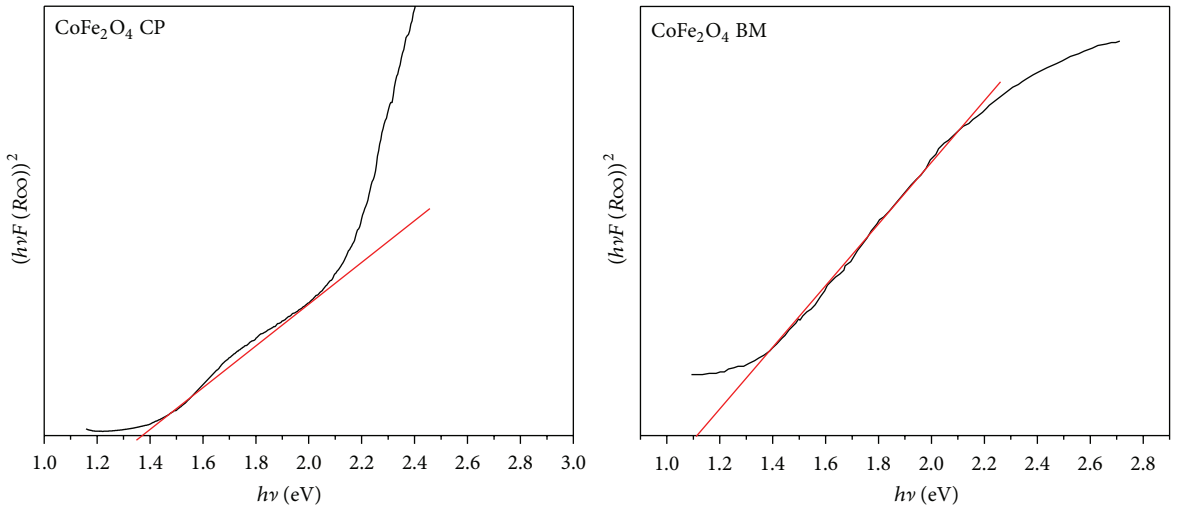

FIGURE 8: UV/Vis diffuse reflectance spectra (indirect transition model) for $CoFe_2O_4$CP and $CoFe_2O_4$BM.

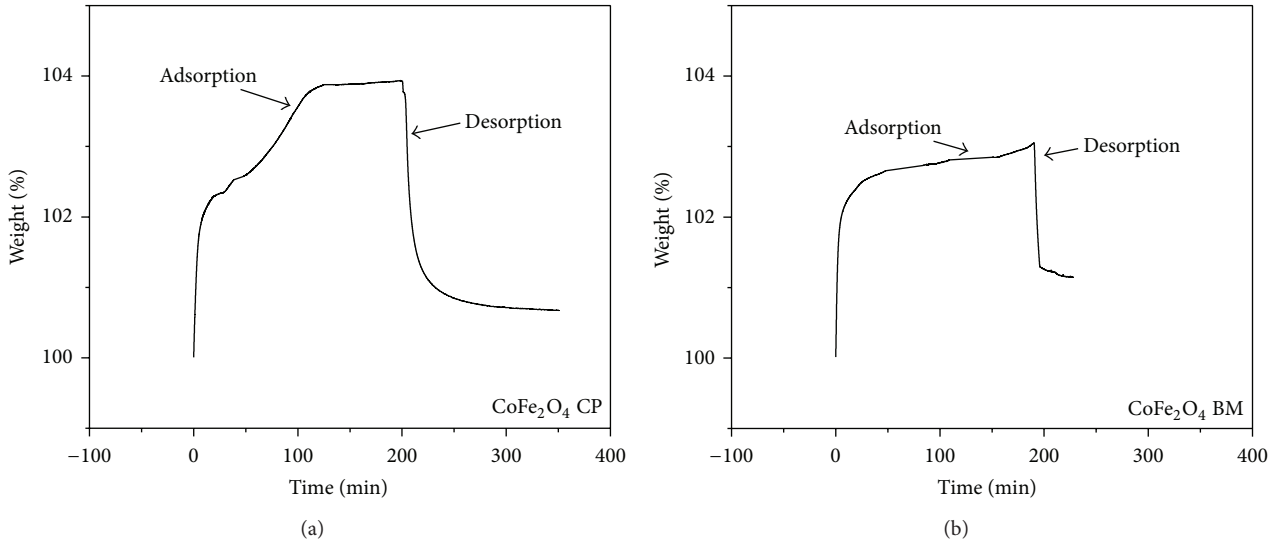

FIGURE 9: Thermogravimetric analysis for the adsorption/desorption of H_2O for samples $CoFe_2O_4$ CP (a) and $CoFe_2O_4$ BM (b).

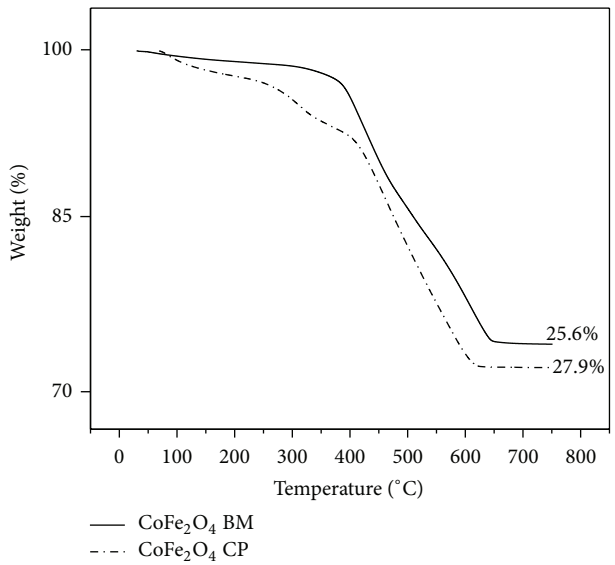

Figure 10: Weight loss of each sample due to oxygen release through the reduction of the ferrites.

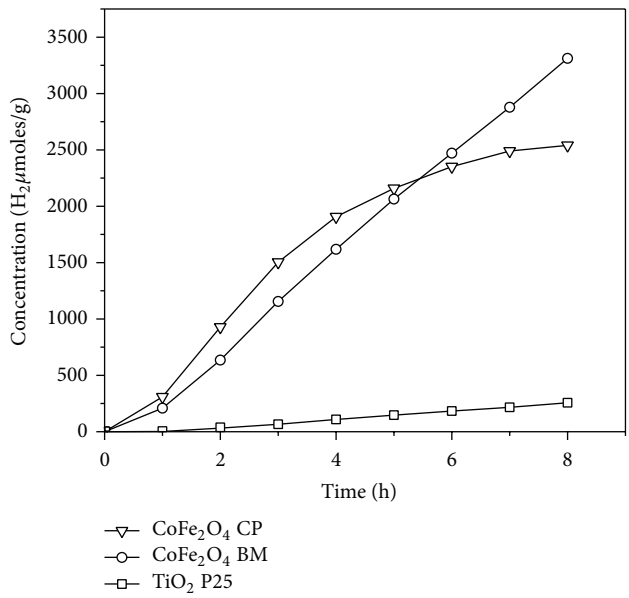

Figure 11: H_2 production per mass of photocatalyst after 8 hours of irradiation for samples $CoFe_2O_4$CP, $CoFe_2O_4$BM, and TiO_2 P25.

to ball milling process. Thus, as the density of the vacancies increases due to collisions during ball milling process, these vacancies presumably generate a material that presents higher water adsorption capacity.

3.7. O_2 Content by TGA. In order to evaluate presence of oxygen vacancies in the synthetized $CoFe_2O_4$, which are related to the amount of O_2 present within each sample, TGA tests were carried out under 5% H_2 atmosphere balance N_2.

Figure 10 shows weight loss of each sample due to oxygen release through the reduction of the ferrite.

The theoretical amount of O_2 released by the complete reduction of $CoFe_2O_4$ is of 27.3%W. In this figure, it can be seen that $CoFe_2O_4$ CP exhibited a slight higher weight loss (27.9%W) than the theoretical value; this can be attributed to the presence of a small amount of Fe_2O_3, which can be responsible for this small increase while the lower weight loss (25.6%W) that $CoFe_2O_4$ BM undergoes can be associated with an important amount of oxygen vacancies that were generated during the ball milling of this material.

3.8. Photocatalytic Evaluation. Figure 11 shows results of the photocatalytic evaluation per mass of photocatalyst after 8 hours of irradiation for the synthetized samples and TiO_2 P25 (reference commercial photocatalyst). In this figure, the hydrogen evolution in μmol/g versus time is plotted.

An analysis of Figure 11 indicates that the photocatalytic activity towards hydrogen production after 8 hours of irradiation for sample $CoFe_2O_4$ CP exhibited about 2540 μmol/g, whereas the activity for sample $CoFe_2O_4$ BM was 3490 μmol/g. Photocatalytic hydrogen from TiO_2 P25 under the same irradiation time was only 250 μmol/g. This behavior can be attributed to the fact that the irradiation energy employed during the experiment was lower than the one needed to activate the TiO_2 P25 sample.

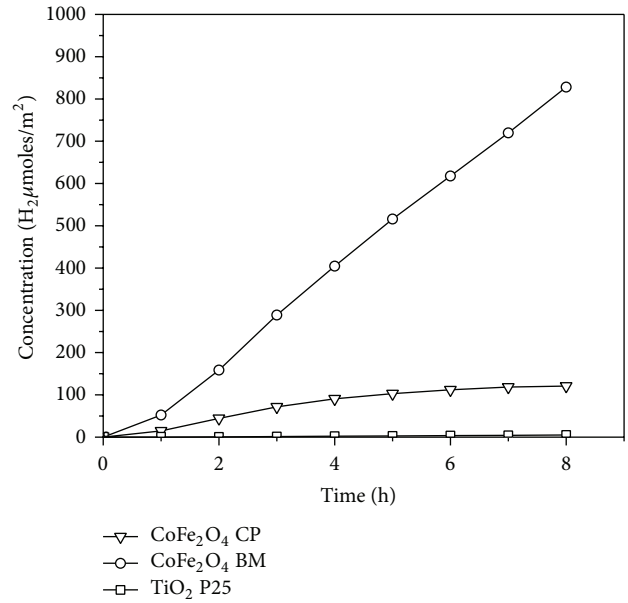

Figure 12: H_2 production per specific surface area of photocatalyst after 8 hours of irradiation for samples $CoFe_2O_4$CP, $CoFe_2O_4$BM, and TiO_2 P25.

Although both samples can be activated under visible light, photoactivity results can be explained in terms of the morphological, textural, chemical, and surface properties that each synthesis method generates on these ferrites.

The behavior toward hydrogen production by the ferrites observed during the first five hours of irradiation indicates that $CoFe_2O_4$CP presents a higher production rate than that of the $CoFe_2O_4$BM. This behavior can be explained in terms of the specific surface area of each material.

Figure 12 shows results of the photocatalytic evaluation per specific surface area of photocatalyst after 8 hours of

irradiation for the synthetized samples and TiO_2 P25 (reference commercial photocatalyst).

In this figure, it can be observed that when applying the area effect to the photocatalytic hydrogen production, the production rate for sample $CoFe_2O_4$BM is significantly higher than that exhibited by $CoFe_2O_4$CP during the entire irradiation time. These results confirm the relevance of the available surface area for the photoactivation and for all other surface phenomena involved during the catalytic water splitting reaction, such as adsorption.

Moreover, the superior photocatalytic activity of sample $CoFe_2O_4$ BM compared to $CoFe_2O_4$ CP can be explained by the findings of Zhang et al. [23] and Geng et al. [24] who reported that the mechanical milling causes a significant increase of vacancies in the solid sample. Thus, a greater amount of hydrogen can be produced due to a high water adsorption capacity of the material. This adsorption capacity presumably can be associated with oxygen vacancies within the material.

It is important to address that even though some studies are reported for the photocatalytic degradation of contaminants and dyes, so far no studies have been reported using $CoFe_2O_4$ for the production of hydrogen, which makes the activity of this material a significant finding [25, 26].

4. Conclusions

Cobalt ferrite was successfully synthesized through two different techniques ($CoFe_2O_4$CP and $CoFe_2O_4$BM), one by chemical coprecipitation and the other by mechanical milling. These materials presented a band gap energy within the visible light range, 1.38 and 1.15 eV, respectively, both exhibiting photocatalytic activity towards hydrogen production. However, sample $CoFe_2O_4$BM has better photocatalytic activity compared to $CoFe_2O_4$CP, which is explained by a high water adsorption capacity of $CoFe_2O_4$BM. This adsorption capacity presumably can be associated with oxygen vacancies within the material.

This greater water adsorption capacity related to oxygen vacancies present in the ferrite obtained by ball milling results in a better photocatalytic activity (3490 μmol g^{-1}) than that synthetized through chemical coprecipitation $CoFe_2O_4$CP (2540 μmol g^{-1}). Even though cobalt ferrite has been used in studies for the photocatalytic degradation of organic pollutants; up to date no studies have reported the use of $CoFe_2O_4$ for the production of hydrogen under visible light irradiation, which makes the activity found for this material a significant finding.

Conflict of Interests

The authors declare that there is no conflict of interests regarding the publication of this paper.

Acknowledgments

The authors acknowledge the help of the laboratories of X-ray diffraction, scanning electron microscopy, transmission electron microscopy, and catalysis during the progress of the present research. Their sincere thanks are due to the Research Center for Advanced Materials (CIMAV) and to the National Council for Science and Technology (CONACYT) for the financial support granted.

References

[1] A. Steinfeld, "Solar hydrogen production via a two-step water-splitting thermochemical cycle based on Zn/ZnO redox reactions," *International Journal of Hydrogen Energy*, vol. 27, no. 6, pp. 611–619, 2002.

[2] R. Fernández-Saavedra, M. B. Gómez-Mancebo, C. Caravaca, M. Sánchez, A. J. Quejido, and A. Vidal, "Hydrogen production by two-step thermochemical cycles based on commercial nickel ferrite: kinetic and structural study," *International Journal of Hydrogen Energy*, vol. 39, no. 13, pp. 6819–6826, 2014.

[3] A. H. McDaniel, A. Ambrosini, E. N. Coker et al., "Nonstoichiometric perovskite oxides for solar thermochemical H_2 and CO production," *Energy Procedia*, vol. 49, pp. 2009–2018, 2014.

[4] F. Fresno, R. Fernández-Saavedra, M. Belén Gómez-Mancebo et al., "Solar hydrogen production by two-step thermochemical cycles: evaluation of the activity of commercial ferrites," *International Journal of Hydrogen Energy*, vol. 34, no. 7, pp. 2918–2924, 2009.

[5] N. Gokon, H. Murayama, A. Nagasaki, and T. Kodama, "Thermochemical two-step water splitting cycles by monoclinic ZrO_2-supported $NiFe_2O_4$ and Fe_3O_4 powders and ceramic foam devices," *Solar Energy*, vol. 83, no. 4, pp. 527–537, 2009.

[6] I. Akkerman, M. Janssen, J. Rocha, and R. H. Wijffels, "Photobiological hydrogen production: photochemical efficiency and bioreactor design," *International Journal of Hydrogen Energy*, vol. 27, no. 11-12, pp. 1195–1208, 2002.

[7] E. Eroglu and A. Melis, "Photobiological hydrogen production: recent advances and state of the art," *Bioresource Technology*, vol. 102, no. 18, pp. 8403–8413, 2011.

[8] I. Akkerman, M. Janssen, J. Rocha, and R. H. Wijffels, "Photobiological hydrogen production: photochemical efficiency and bioreactor design," *International Journal of Hydrogen Energy*, vol. 27, no. 11-12, pp. 1195–1208, 2002.

[9] O. Kubo, T. Ido, and H. Yokoyama, "Properties of Ba ferrite particles for perpendicular magnetic recording media," *IEEE Transactions on Magnetics*, vol. 18, no. 6, pp. 1122–1124, 1982.

[10] R. Valenzuela, *Magnetic Ceramics*, Cambridge University Press, Cambridge, UK, 1st edition, 1994.

[11] V. Hays, R. Marchand, G. Saindrenan, and E. Gaffet, "Nanocrystalline Fe-Ni solid solutions prepared by mechanical alloying," *Nanostructured Materials*, vol. 7, no. 4, pp. 411–420, 1996.

[12] N. M. Deraz, "Production and characterization of pure and doped copper ferrite nanoparticles," *Journal of Analytical and Applied Pyrolysis*, vol. 82, no. 2, pp. 212–222, 2008.

[13] H. Yang, J. Yan, Z. Lu, X. Cheng, and Y. Tang, "Photocatalytic activity evaluation of tetragonal $CuFe_2O_4$ nanoparticles for the H_2 evolution under visible light irradiation," *Journal of Alloys and Compounds*, vol. 476, no. 1-2, pp. 715–719, 2009.

[14] A. Kezzim, N. Nasrallah, A. Abdi, and M. Trari, "Visible light induced hydrogen on the novel hetero-system $CuFe_2O_4/TiO_2$," *Energy Conversion and Management*, vol. 52, no. 8-9, pp. 2800–2806, 2011.

[15] X. Hu, P. Guan, and X. Yan, "Hydrothermal synthesis of nanometer microporous zinc ferrite," *China Particuology*, vol. 2, no. 3, pp. 135–137, 2004.

[16] N. Duman, M. V. Akdeniz, and A. O. Mekhrabov, "Magnetic monitoring approach to nanocrystallization kinetics in Fe-based bulk amorphous alloy," *Intermetallics*, vol. 43, pp. 152–161, 2013.

[17] A. H. Hamid and A. Abolghasem, "Investigation on phase evolution in the processing of nano-crystalline cobalt ferrite by solid-state reaction route," *Advanced Materials Research*, vol. 829, pp. 767–771, 2014.

[18] M. Ristić, B. Hannoyer, S. Popović, S. Musić, and N. Bajraktaraj, "Ferritization of copper ions in the Cu-Fe-O system," *Materials Science and Engineering B: Solid-State Materials for Advanced Technology*, vol. 77, no. 1, pp. 73–82, 2000.

[19] Z. Zi, Y. Sun, X. Zhu, Z. Yang, J. Dai, and W. Song, "Synthesis and magnetic properties of $CoFe_2O_4$ ferrite nanoparticles," *Journal of Magnetism and Magnetic Materials*, vol. 321, no. 9, pp. 1251–1255, 2009.

[20] Y. Cedeño-Mattei, O. Perales-Pérez, and O. N. C. Uwakweh, "Effect of high-energy ball milling time on structural and magnetic properties of nanocrystalline cobalt ferrite powders," *Journal of Magnetism and Magnetic Materials*, vol. 341, pp. 17–24, 2013.

[21] X. Limei, F. Zhang, C. Bin, X. B. Chen, and X. Bai, "Preparation of light-driven spinel nanoparticles $CoAl_2O_4$, $MgFe_2O_4$ and $CoFe_2O_4$ and their photocatalytic reduction of carbon dioxide," in *Proceedings of the International Conference on Computer Distributed Control and Intelligent Environmental Monitoring (CDCIEM '11)*, pp. 2153–2156, Changsha, China, 2011.

[22] S. M. Chavan, M. K. Babrekar, S. S. More, and K. M. Jadhav, "Structural and optical properties of nanocrystalline Ni-Zn ferrite thin films," *Journal of Alloys and Compounds*, vol. 507, no. 1, pp. 21–25, 2010.

[23] B. Q. Zhang, L. Lu, and M. O. Lai, "Evolution of vacancy densities in powder particles during mechanical milling," *Physica B: Condensed Matter*, vol. 325, pp. 120–129, 2003.

[24] Y. Geng, T. Ablekim, P. Mukherjee, M. Weber, K. Lynn, and J. E. Shield, "High-energy mechanical milling-induced crystallization in $Fe_{32}Ni_{52}Zr_3B_{13}$," *Journal of Non-Crystalline Solids*, vol. 404, pp. 140–144, 2014.

[25] P. H. Borse, C. R. Cho, K. T. Lim et al., "Synthesis of barium ferrite for visible light photocatalysis applications," *Journal of the Korean Physical Society*, vol. 58, no. 6, pp. 1672–1676, 2011.

[26] E. Casbeer, V. K. Sharma, and X.-Z. Li, "Synthesis and photocatalytic activity of ferrites under visible light: a review," *Separation and Purification Technology*, vol. 87, pp. 1–14, 2012.

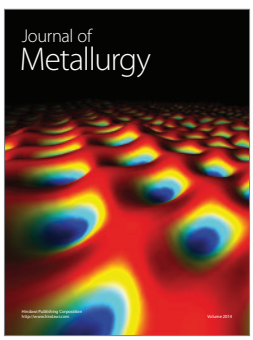

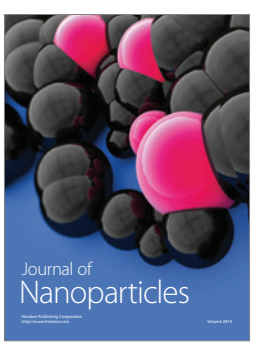

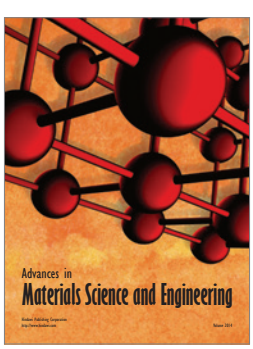

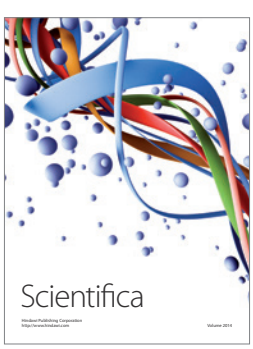

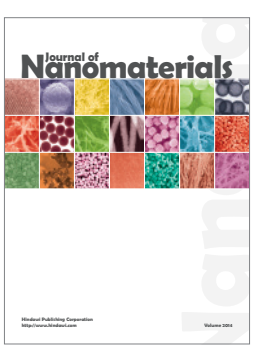

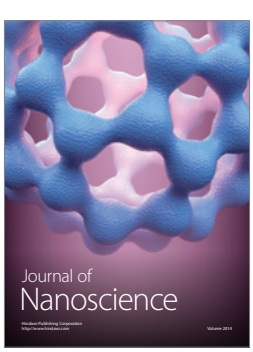

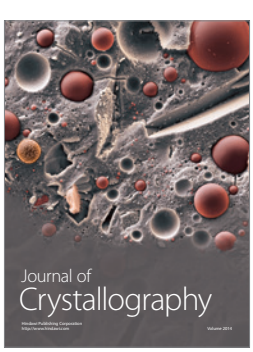

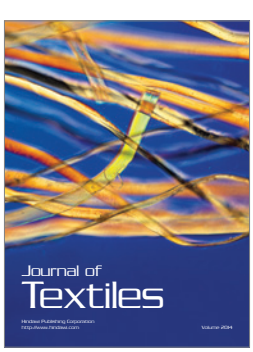

Hindawi

Submit your manuscripts at
http://www.hindawi.com